Chemical control of structure and guest uptake by a conformationally mobile porous material

Alexandros P. Katsoulidis, Dmytro Antypov, George F. S. Whitehead, Elliot J. Carrington, Dave J. Adams[1], Neil G. Berry, George R. Darling, Matthew S. Dyer and Matthew J. Rosseinsky*
Department of Chemistry, University of Liverpool, Liverpool L69 7ZD

Metal–organic frameworks (MOFs) are crystalline synthetic porous materials formed by binding organic linkers to metal nodes: they can be either rigid[1,2] or flexible.[3] Zeolites and rigid MOFs have widespread applications in sorption, separation and catalysis that arise from their ability to control the arrangement and chemistry of guests in their pores via the shape and functionality of the internal surface defined by their chemistry and structure.[4,5] Their structures correspond to an energy landscape with a single, albeit highly functional, energy minimum. In contrast, proteins function by navigating between multiple metastable structures using bond rotations of the polypeptide,[6,7] where each structure lies in one of the minima of a conformational energy landscape and can be selected according to the chemistry of the molecules interacting with the protein. These structural changes are realised through the mechanisms of conformational selection (where a higher energy minimum characteristic of the protein is stabilised by small molecule binding), and induced fit (where a small molecule imposes a structure on the protein that is not a minimum in the absence of that molecule).[8] Here we show that rotation about covalent bonds in a peptide linker can change a flexible MOF to afford nine distinct crystal structures, revealing a conformational energy landscape characterised by multiple structural minima. The uptake of small molecule guests by the MOF can be chemically triggered by inducing peptide conformational change. This change transforms the material from a minimum on the landscape that is inactive for guest sorption to an active one. Chemical control of the conformation of a flexible organic linker offers a route to modify the pore geometry and internal surface chemistry and thus the function of open-framework materials.

Flexible MOF structures[9,10] can be rearranged in the presence of guests through mechanical mechanisms such as the repositioning of a rigid linker about an inorganic unit[11-13] or the relative displacement of two rigid networks,[14] opening a range of routes to control function[15] that are not accessible to rigid frameworks with their single structural minimum (Figure 1). Similar phenomena have been observed in the host-guest chemistry of interlocked cage molecules.[16-18] Alternatively, rotations about bonds involving sp^3 carbons[19-25] allow MOF to access different structures. For example, low energy conformational changes of dipeptide Gly-X linkers produce open and closed forms of $Zn(Gly\text{-}X)_2$ frameworks.[26,27] The greater chemical diversity and more complex conformational space of higher order oligopeptides offer MOF with multiple open structures (Figure 1). This could allow interaction with molecules in the pores to select a specific structure for a defined function from the resulting energy landscape. That structure would be accessed through the single bond rotation pathway used by proteins (Figure 1).

The tripeptide glycine-glycine-L-histidine (GGH) affords a three-dimensional chiral MOF ZnGGH-1•($DMF\text{-}H_2O$) by deprotonation of both the C-terminal acid and the imidazole function of the His sidechain that produces a tetratopic linker, which coordinates to Zn^{2+}

[1] Present address: School of Chemistry, Joseph Black Building, University of Glasgow, Glasgow G12 8QQ, UK

(Figure 1b and Extended Data Fig. 1). ZnGGH-1•(DMF-H_2O) displays one-dimensional pores that contain one DMF and 0.85 H_2O per formula unit (Supplementary Note 1). It is comprised of rigid Zn-His layers connected by the conformationally mobile Gly-Gly chain, which confers flexibility on the framework (Extended Data Fig. 1b). ZnGGH-1•(DMF-H_2O) is isoreticular to ZnCar•DMF[28], which is based on the dipeptide carnosine (Car, beta-alanyl-L-histidine), with a wider pore window of 4.9 Å and similar chemical stability in a variety of solvents including water, attributed to the Zn-imidazolate bonds. The combination of chemical functionalisation of the internal surface and the flexible Gly-Gly component of the tripeptide allows the structure of the ZnGGH framework to respond sensitively to the presence, shape and chemistry of the species in the pores, which in turn controls chemical function. For example, dioxane and cyclopentanol guests are not adsorbed by DMSO-solvated ZnGGH, however the exchange of DMSO solvent from the pores with DMF triggers the adsorption of these guests (Figure 2 and Extended Data Fig. 2).

To understand this triggered adsorption, we explored how the structure of the ZnGGH framework can be controlled through non-covalent interactions with polar solvents DMF, H_2O, MeOH and DMSO (Extended Data Fig. 2 and Supplementary Note 2) and how the pore content affects sorption of larger guests such as dioxane, cyclopentanol, furfural (F) and furfuryl alcohol (FA). A series of adsorption experiments showed that these guests can be adsorbed by ZnGGH in the presence of any solvent in the pores except DMSO (Table S5). Powder X-ray diffraction (PXRD) data show that the treatment of ZnGGH-1•(DMF-H_2O) with DMSO produces a new structure, ZnGGH-2•(DMSO), which does not adsorb guests even if they are the only component in the liquid phase, *e.g.,* neat dioxane does not access the pores of ZnGGH-2•(DMSO), although it does access the pores of ZnGGH-1•(DMF-H_2O). However, the pores of ZnGGH-2•(DMSO) are accessible to solvents such as DMF and H_2O, which exchange DMSO and transform the structure to the new structures ZnGGH-3•(DMF) and ZnGGH-4•(H_2O) respectively. Guests are adsorbed in significant quantity by these distinct new structures (Table S5). Specifically, addition of an equimolar liquid mixture of dioxane and DMF to ZnGGH-3•(DMF) affords ZnGGH-1, where the pore species are (dioxane:DMF:GGH = 0.5:0.33:1). These adsorption results reveal that there are solvated ZnGGH structures that are either active for adsorption of dioxane and cyclopentanol, such as ZnGGH-1•(DMF-H_2O), ZnGGH-3•(DMF) and ZnGGH-4•(H_2O), or inactive, such as ZnGGH-2•(DMSO). Addition of 0.1 moles of DMF to a suspension of ZnGGH-2•(DMSO) in 0.1 moles of dioxane changes the structure and triggers the adsorption of dioxane. After this process, the pores primarily contain dioxane (dioxane:DMF:DMSO:GGH = 0.47:0.26:0.11:1) and the structure corresponds to ZnGGH-1 (Figure 2 and Extended Data Fig. 2b). No intermediate phases are observed during the structure transformation by PXRD (Figures S29 – S35).

The differences in the guest adsorption behaviour of these solvated structures are ascribed to the changes in pore size and shape and non-covalent bonding patterns revealed by their structures. Crystals of eight solvated ZnGGH structures were obtained by soaking the as-made material, ZnGGH-1•(DMF-H_2O), in different solvents and guests (Extended Data Fig. 2a). All structures were analysed by single crystal X-ray diffraction (SCXRD) and their phase purity confirmed by PXRD. In each structure, the peptide linker adopts a distinct conformation by readjusting its torsions (Figure S16) to respond to the pore species within the ZnGGH framework. The bond showing the most diverse rotational states is the N-C_a of the central Gly whose torsion φ_1, C-N-C_a-C, changes by 156° between the nine different observed structures, relocating the N-terminal Gly (Figure 3a). In ZnGGH-2•(DMSO) the linker is twisted (φ_1 = 268°), directing the Gly-Gly amide group inside the pore to form a hydrogen bond with DMSO, and positioning the terminal NH_2 to hydrogen bond with the Gly-His amide of the adjacent linker (Figure 3b, c and Extended Data Fig. 3). This structure exhibits the smallest solvent accessible volume and pore window of 4.5 Å of all the ZnGGH structures (Extended Data

Table 1). Exchange of DMSO with DMF changes the torsion about the N-C_a bond of the central Gly by 135° (φ_1 = 133°). This peptide conformation aligns the Gly-Gly amide groups along the pore walls to form an antiparallel beta sheet-like hydrogen bond network between adjacent linkers and positions the terminal NH_2 group to hydrogen bond to DMF (Figure 3b, c). The resulting ZnGGH-3•(DMF) has the largest pore window (5.4 Å). In ZnGGH-1•(DMF-H_2O) the linker adopts an intermediate conformation (φ_1 = 180°) that enables the terminal NH_2 to hydrogen bond both to the Gly-His amide of the adjacent linker and to DMF, which adopts an orthogonal orientation to that in ZnGGH-3•(DMF) (Extended Data Fig. 4). Collapsed ZnGGH-9 is obtained by removing the solvent from any of the above compounds. The peptide linker folds predominantly around the φ_2 torsion of His and the ψ torsion of the central Gly to remove the extra-framework space, which results in two very similar conformations (Extended Data Fig. 5). All the above materials demonstrate that the ZnGGH framework readily transforms its structure through changes in peptide conformation driven by the chemistry in its pores.

Dihedral angle principal component analysis, dPCA, is used to reduce the dimensions of the conformational energy landscape of proteins and thus enable understanding of the structural changes driven by interactions with small molecules.[29] dPCA was applied to all the experimentally observed linker conformations in ZnGGH and reveals three clusters: straight, twisted and folded (Figure 4a and Extended Data Fig. 6a). The straight cluster includes those conformations giving the six most porous structures including ZnGGH-1 and ZnGGH-3. There are noticeable differences between these conformations (Extended Data Fig. 6b), which were further analysed by a separate dPCA that identified four subgroups within the straight cluster (Figure 4b). These subgroups separate materials which, despite apparently similar pore content, differ in hydrogen bonding, such as ZnGGH-1•(DMF-H_2O), ZnGGH-3•(DMF) and ZnGGH-5•(H_2O-DMF) (Extended Data Fig. 7), and the pair of structures containing the furanic guests ZnGGH-6•(Furfural) and ZnGGH-7•(Furfuryl alcohol) (Extended Data Fig. 8). The second cluster contains linker conformations that have been twisted around the φ_1 torsion of the central Gly, as found in the less porous DMSO-solvated structure ZnGGH-2. The third cluster contains the folded conformations observed only in the collapsed structure ZnGGH-9. ZnGGH-4, observed in water, methanol and formamide, displays alternating straight and twisted linkers and is the only structure with peptide conformations belonging to two clusters (Figure 4a and Extended Data Fig. 9).

For each of the nine experimentally-observed systems, we optimised the host structure in the absence of molecules in the pores using density functional theory (DFT). All of them, except ZnGGH-4, converged to one of three calculated empty structures. Each of these three structures corresponds directly to one of the three linker conformation clusters identified in the dPCA. The six different experimental structures (Figure 4b) in the straight linker conformation cluster all converge to the same empty structure when optimised. The three calculated structures, *S-ZnGGH* for the straight conformation cluster, *T-ZnGGH* for the twisted and *F-ZnGGH* for the folded, shown as solid circles coloured according to their energy in Fig. 4a, are three local minima on the conformational energy landscape of the empty host that underlie the clustering of the solvated host structures observed experimentally. These local minima are characteristic of the ZnGGH framework itself and they are separated by energy barriers associated with the large conformational changes within the host that characterise the three different clusters. Transition paths computed between the three calculated structures show that folding and twisting of the straight linker conformation requires crossing barriers of 12.4 kJ/mol and 19.5 kJ/mol respectively (Figure 4a), typical for fast folding proteins.[30] The barriers correspond to experimentally observed two-phase coexistence, for instance of ZnGGH-2 and ZnGGH-3 structures in the presence of DMSO/DMF mixtures (Figure S15). It is possible to experimentally access energy minima of ZnGGH that are not observed on the conformational energy landscape of the empty framework through their stabilisation by guests. The empty

ZnGGH-4, which uniquely displays two linker conformations belonging to distinct clusters, was found to be unstable upon energy minimization, but stable in the presence of a water molecule or a methanol molecule that forms two hydrogen bonds with the framework, as observed experimentally. This suggests that, unlike all the other structures, ZnGGH-4 is not characteristic of the ZnGGH framework itself, but is stabilised by specific interactions with the guests through an induced fit mechanism analogous to that used by proteins.

The adoption of a structure in one of the three local minima on the conformational energy landscape of empty ZnGGH is driven by reordering of their energy ranking by the molecule occupying the pores and can be considered as conformational selection of that minimum. Addition of DMF in the presence of dioxane or cyclopentanol to ZnGGH-2•(DMSO) removes DMSO and selects the straight linker conformation (Figure 4c). This transforms ZnGGH from the twisted linker minimum *T-ZnGGH* that is inactive for dioxane or cyclopentanol uptake, to the active straight linker minimum *S-ZnGGH*, and enables the uptake of the dioxane and cyclopentanol guests. These chemically triggered conformational changes of peptides modify the structure and thus control the functional behaviour of the porous ZnGGH framework.

References

1 Furukawa, H., Cordova, K. E., O'Keeffe, M. & Yaghi, O. M. The Chemistry and Applications of Metal-Organic Frameworks. *Science* **341**, (2013).

2 Howarth, A. J. *et al.* Chemical, thermal and mechanical stabilities of metal–organic frameworks. *Nature Reviews Materials* **1**, 15018, (2016).

3 Kitagawa, S., Kitaura, R. & Noro, S.-i. Functional Porous Coordination Polymers. *Angewandte Chemie International Edition* **43**, 2334-2375, (2004).

4 Moliner, M., Martínez, C. & Corma , A. Multipore Zeolites: Synthesis and Catalytic Applications. *Angewandte Chemie International Edition* **54**, 3560-3579, (2015).

5 Kaskel, S. in *The Chemistry of Metal–Organic Frameworks* 1-3 (Wiley-VCH Verlag GmbH & Co. KGaA, 2016).

6 Beck, D. A. C., Alonso, D. O. V., Inoyama, D. & Daggett, V. The intrinsic conformational propensities of the 20 naturally occurring amino acids and reflection of these propensities in proteins. *Proceedings of the National Academy of Sciences* **105**, 12259-12264, (2008).

7 Swain, J. F. & Gierasch, L. M. The changing landscape of protein allostery. *Current Opinion in Structural Biology* **16**, 102-108, (2006).

8 Csermely, P., Palotai, R. & Nussinov, R. Induced fit, conformational selection and independent dynamic segments: an extended view of binding events. *Trends in Biochemical Sciences* **35**, 539-546, (2010).

9 Schneemann, A. *et al.* Flexible metal-organic frameworks. *Chemical Society Reviews* **43**, 6062-6096, (2014).

10 Horike, S., Shimomura, S. & Kitagawa, S. Soft porous crystals. *Nat Chem* **1**, 695-704, (2009).

11 Loiseau, T. *et al.* A Rationale for the Large Breathing of the Porous Aluminum Terephthalate (MIL-53) Upon Hydration. *Chemistry – A European Journal* **10**, 1373-1382, (2004).

12 Nouar, F. *et al.* Tuning the breathing behaviour of MIL-53 by cation mixing. *Chemical Communications* **48**, 10237-10239, (2012).

13 Serre, C. *et al.* Role of Solvent-Host Interactions That Lead to Very Large Swelling of Hybrid Frameworks. *Science* **315**, 1828-1831, (2007).

14 Maji, T. K., Matsuda, R. & Kitagawa, S. A flexible interpenetrating coordination framework with a bimodal porous functionality. *Nat Mater* **6**, 142-148, (2007).

15 Mason, J. A. *et al.* Methane storage in flexible metal–organic frameworks with intrinsic thermal management. *Nature* **527**, 357-361, (2015).

16 Sabrina, F. *et al.* Allosteric Binding of Halide Anions by a New Dimeric Interpenetrated Coordination Cage. *Angewandte Chemie International Edition* **51**, 2191-2194, (2012).
17 Freye, S. *et al.* Template Control over Dimerization and Guest Selectivity of Interpenetrated Coordination Cages. *Journal of the American Chemical Society* **135**, 8476-8479, (2013).
18 Löffler, S. *et al.* Triggered Exchange of Anionic for Neutral Guests inside a Cationic Coordination Cage. *Journal of the American Chemical Society* **137**, 1060-1063, (2015).
19 Lin, Z.-J., Lu, J., Hong, M. & Cao, R. Metal-organic frameworks based on flexible ligands (FL-MOFs): structures and applications. *Chemical Society Reviews* **43**, 5867-5895, (2014).
20 Colodrero, R. M. P. *et al.* Multifunctional lanthanum tetraphosphonates: Flexible, ultramicroporous and proton-conducting hybrid frameworks. *Dalton Transactions* **41**, 4045-4051, (2012).
21 Rouschmeyer, P. *et al.* A Flexible Fluorescent Zr Carboxylate Metal–Organic Framework for the Detection of Electron-Rich Molecules in Solution. *Inorganic Chemistry* **56**, 8423-8429, (2017).
22 H.-M. Yeung, H., Kosa, M., Parrinello, M. & Cheetham, A. K. Chiral, Racemic, and Meso-Lithium Tartrate Framework Polymorphs: A Detailed Structural Analysis. *Crystal Growth & Design* **13**, 3705-3715, (2013).
23 Motkuri, R. K. *et al.* Role of hydrocarbons in pore expansion and contraction of a flexible metal-organic framework. *Chemical Communications* **47**, 7077-7079, (2011).
24 Murdock, C. R., Lu, Z. & Jenkins, D. M. Effects of Solvation on the Framework of a Breathing Copper MOF Employing a Semirigid Linker. *Inorganic Chemistry* **52**, 2182-2187, (2013).
25 Haddad, J., Whitehead, G. F. S., Katsoulidis, A. P. & Rosseinsky, M. J. In-MOFs based on amide functionalised flexible linkers. *Faraday Discussions* **201**, 327-335, (2017).
26 Rabone, J. *et al.* An Adaptable Peptide-Based Porous Material. *Science* **329**, 1053-1057, (2010).
27 Martí Gastaldo, C. *et al.* Side-chain control of porosity closure in single- and multiple-peptide-based porous materials by cooperative folding. *Nat Chem* **6**, 343-351, (2014).
28 Katsoulidis, A. P. *et al.* Guest-Adaptable and Water-Stable Peptide-Based Porous Materials by Imidazolate Side Chain Control. *Angewandte Chemie International Edition* **53**, 193-198, (2014).
29 Mu, Y., Nguyen, P. H. & Stock, G. Energy landscape of a small peptide revealed by dihedral angle principal component analysis. *Proteins: Structure, Function, and Bioinformatics* **58**, 45-52, (2005).
30 Naganathan, A. N., Sanchez-Ruiz, J. M. & Muñoz, V. Direct Measurement of Barrier Heights in Protein Folding. *Journal of the American Chemical Society* **127**, 17970-17971, (2005).

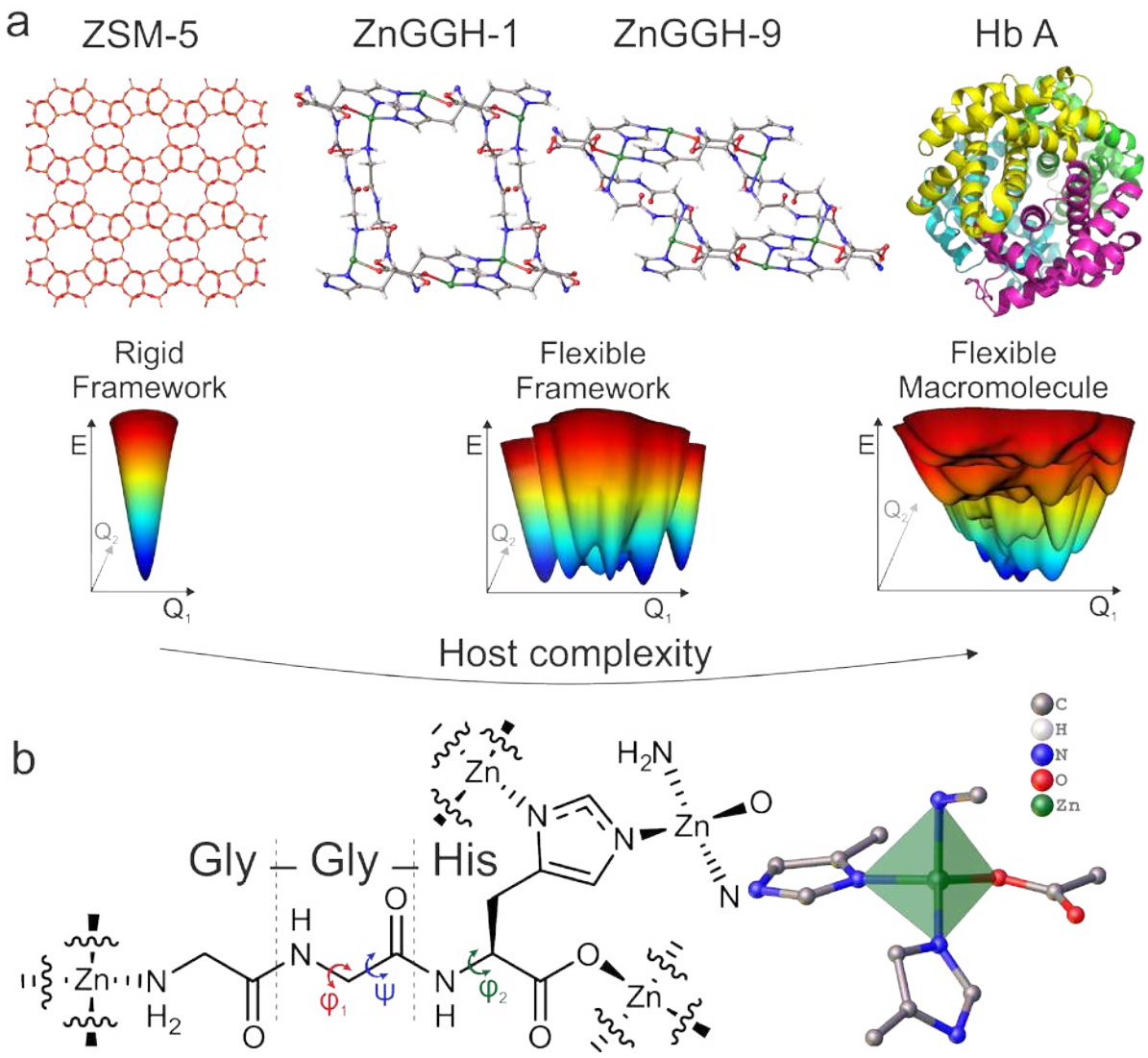

Figure 1 The structural flexibility of ZnGGH in the context of a conformational energy landscape. (a) ZSM-5 is a rigid porous framework and its energy landscape (a representation of energy as a function of the positional degrees of freedom, here Q_1 and Q_2, of the structure) displays one minimum corresponding to a single conformation. The protein Hb A, human haemoglobin, is a flexible macromolecule, which adopts a range of conformations to perform its biological function. Its conformational energy landscape therefore displays multiple minima. The new ZnGGH compound reported here is a flexible porous framework. ZnGGH-1 is the structure of the as-made framework and ZnGGH-9 is the structure of the collapsed framework. The flexibility that connects structures 1 and 9 arises from the conformational degrees of freedom, shown as Q_1 and Q_2, of the peptide linker, as in the case of proteins. ZnGGH can readjust its pore shape and the position of functional groups in the presence of different solvents by changing the peptide conformation, producing eight distinct solvated and one collapsed crystal structure. This gives ZnGGH a conformational energy landscape with multiple minima. In contrast to the macromolecular state of proteins, ZnGGH is a crystalline solid framework, which restricts the available conformational space of the linker. All energy landscapes drawn in this figure are hypothetical illustrations that reflect the structural properties of the corresponding materials. (b) The doubly deprotonated tripeptide Gly-Gly-L-His acts as a tetratopic linker to form the ZnGGH framework, connecting four Zn^{2+} centres.

Each Zn^{2+} is tetrahedrally coordinated by four Gly-Gly-L-His linkers. The highlighted torsions φ_1, ψ, and φ_2 vary significantly between the structures and are referred to in the text.

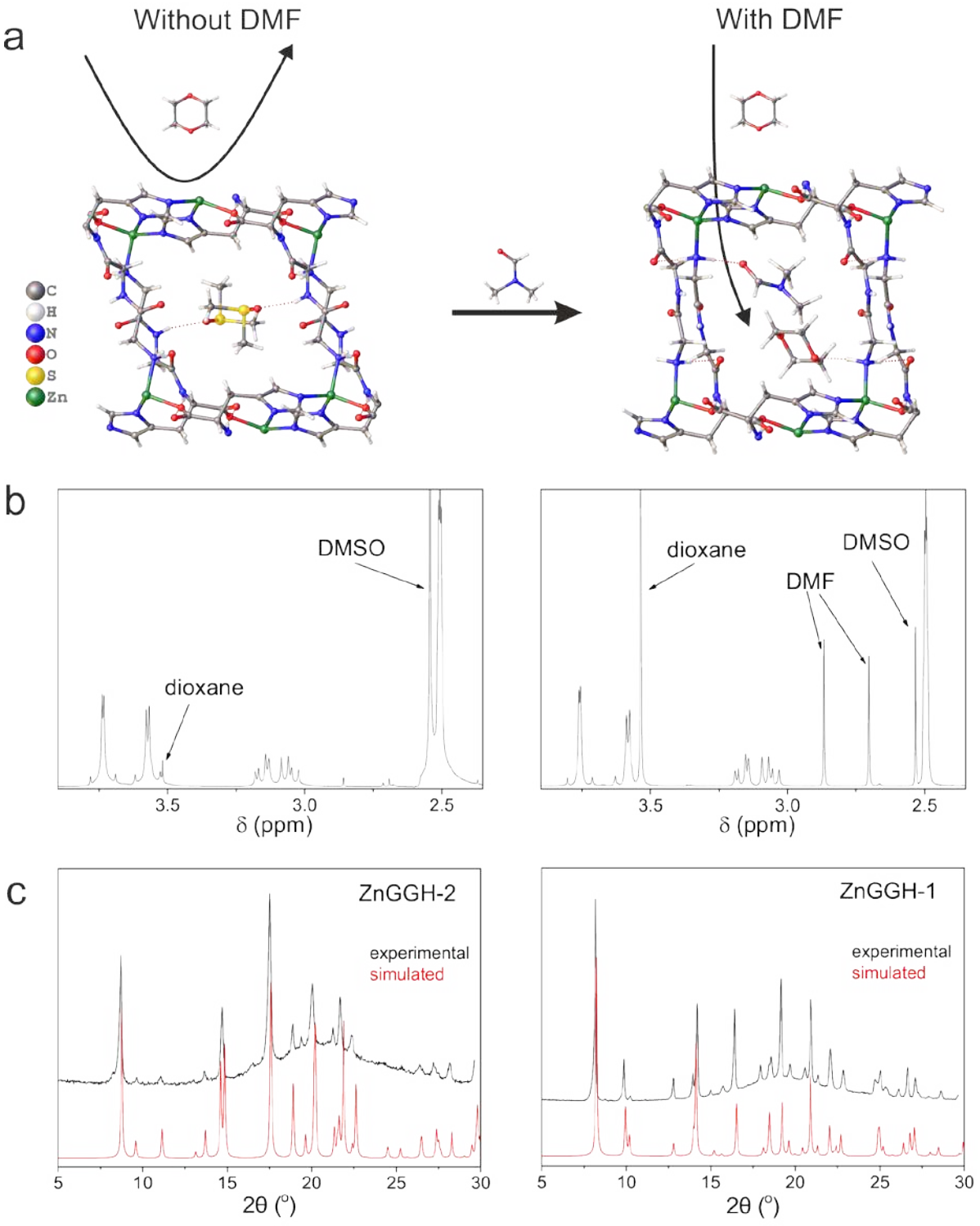

Figure 2 Chemical triggering of guest adsorption. (a) Dioxane is not adsorbed by ZnGGH-2•(DMSO) (left: DMSO occupies the pores, the arrow indicates that dioxane remains in the liquid phase. Single crystal X-ray diffraction shows that the structure is unchanged (Supplementary Note 4). Atomic positions shown are from the refined single crystal structure

of ZnGGH-2•(DMSO)). Addition of DMF (molar ratio DMF:dioxane = 1:1) produces a crystal structure transformation and triggers the adsorption of dioxane (right: DMF and dioxane occupy the pores, the arrow indicates that dioxane transfers from the liquid to the solid phase. Atomic positions shown are from the refined single crystal structure of ZnGGH-1•(DMF-H_2O) in which the positions of one DMF and one dioxane molecule were optimised using DFT). The structural transformation from ZnGGH-2 to ZnGGH-1 is completed in 3 days. The compositional and structural evidence for this is shown below. (b) Left: ^{1}H NMR of ZnGGH-2•(DMSO) following treatment with pure dioxane for four days and subsequent digestion. The composition of this material according to ^{1}H NMR is dioxane:DMSO:GGH = 0.017:0.62:1. Right: Equivalent ^{1}H NMR data when DMF is added to the mixture of dioxane and ZnGGH-2•(DMSO), allowing adsorption of dioxane. The composition of the final product is dioxane:DMF:DMSO:GGH = 0.47:0.26:0.11:1. (c) PXRD patterns (black, measured on the slurry after the experiment) of (left) inactive ZnGGH-2•(DMSO) after the treatment with dioxane for four days and (right) of ZnGGH-1, which is obtained 3 days after the addition of DMF that triggers dioxane adsorption. Both patterns are compared with the simulated patterns (red) from the crystal structures ZnGGH-2•(DMSO) and ZnGGH-1•(DMF-H_2O).

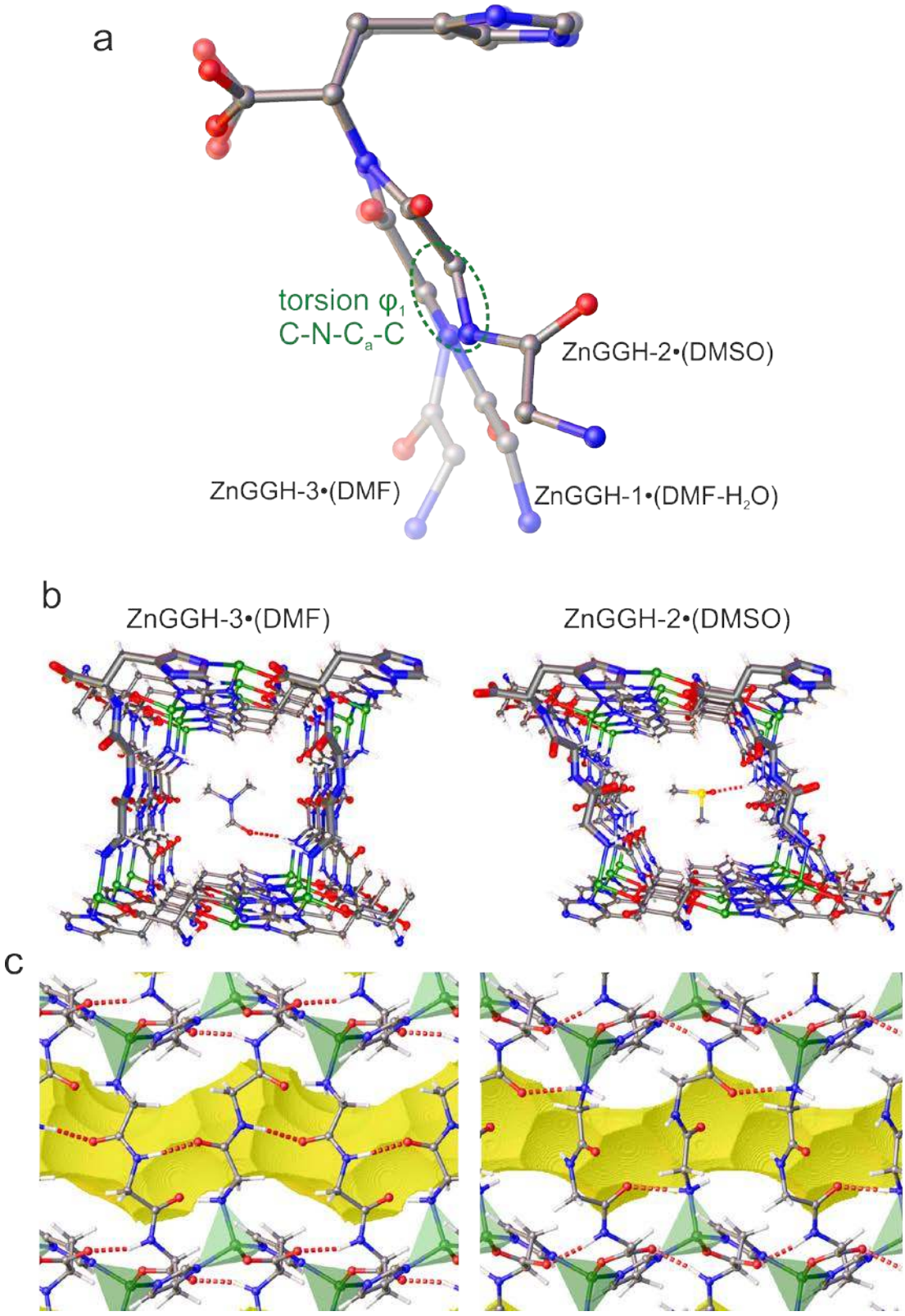

Figure 3 Linker conformation directs pore shape and internal surface chemistry. (a) Conformation of the GGH linker in the refined experimental crystal structures ZnGGH-1•(DMF-H_2O), ZnGGH-2•(DMSO) and ZnGGH-3•(DMF). The different conformations are realised by the diverse torsional states of φ_1 of the central Gly (broken circle). This repositions the N-terminal Gly, affecting the pore shape and the availability of functional groups. (b) The

view down the 1D pores for ZnGGH-3•(DMF) and ZnGGH-2•(DMSO) shows the different pore shapes and the orientation of functional groups. In ZnGGH-3, DMF is hydrogen bonded (dotted line) at the corner of the pore with the terminal NH_2, whereas DMSO in ZnGGH-2 is hydrogen bonded to the Gly-Gly amide group in the middle of the pore wall. (c) The side view reveals the intraframework hydrogen bond pattern for each structure. ZnGGH-3 exhibits antiparallel beta sheet hydrogen bonding between the Gly-Gly amide groups along the pore walls. ZnGGH-2 features hydrogen bonds between the terminal NH_2 and the Gly-His amide of neighbouring linkers. Both structures exhibit hydrogen bonds between the His carboxylate and the Gly-His amide. The Connolly surface (shown in yellow) reveals differences in pore dimensions. ZnGGH-3 displays a pore window of 5.4 Å whereas ZnGGH-2 has a pore window of 4.5 Å.

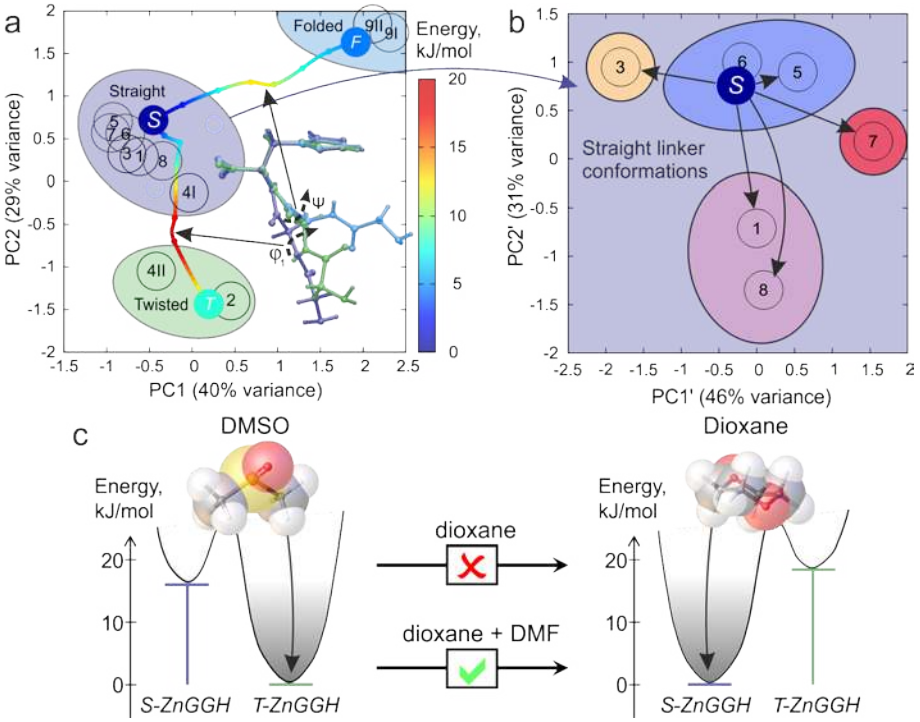

Figure 4 Conformational energy landscape and selection of an active minimum in ZnGGH. Dihedral angle principal component analysis (dPCA) of linker conformations observed in (a) all experimental structures and (b) the six structures within the straight linker cluster in (a). The black circles marked with the number X for each ZnGGH-X structure denote the experimentally observed linker conformations while coloured solid circles correspond to the three pictured linker conformations observed in the calculated empty host structures *S-ZnGGH*, *T-ZnGGH* and *F-ZnGGH*, color-coded according to their energy per linker. The calculated transition paths between these minima represent the conformational energy landscape of ZnGGH. The solid arrows in (a) indicate the positions of energy barriers on the conformational energy landscape and the dashed arrows show the largest change in linker torsions between the calculated structures shown. In (b), four subgroups of experimental structures are identified in the vicinity of the global minimum *S-ZnGGH* on the conformational energy landscape. These subgroups were found to differ in the details of the intra-framework hydrogen bonding (Extended Data Fig. 7 and 8). The black arrows represent the conformational adjustment due to interactions between the framework and the species in the pores that result in the observed ZnGGH-X crystal structures. In (c), the calculated relative energies per linker are shown for ZnGGH with DMSO and dioxane in the pores when their positions are optimised

in a flexible host close to either the *S-ZnGGH* or *T-ZnGGH* minima *i.e.,* with either straight or twisted linkers (Supplementary Note 7). For DMSO the *T-ZnGGH* minimum has the lower energy, in agreement with the experimentally observed structure. Dioxane prefers the *S-ZnGGH* minimum, however experiment shows that it cannot alone drive the transformation from *T-ZnGGH* to *S-ZnGGH*. The addition of DMF is required to select this minimum and allow dioxane uptake.

Supplementary Information
The file contains Supplementary Results (PXRD, TGA, NMR and Crystallographic Tables), Supplementary Notes and Supplementary References.

Acknowledgements
This project has received funding from the European Research Council (ERC) under the European Union's Horizon 2020 research and innovation programme (grant agreement n° 692685) and from the Engineering and Physical Sciences Research Council (EP/J008834). We acknowledge the HPC Materials Chemistry Consortium for providing access to UK's national supercomputer ARCHER under the EPSRC grant EP/L000202. We thank Diamond Light Source for provision of beamtime on the I11 and I19 beamlines and the X-ray crystallography facility of the School of Chemistry at the University of Manchester for the use of their Rigaku Oxford diffraction FR-X instrument to collect two of the single crystal diffraction datasets.

Author contributions
A.P.K., D.A. and M.J.R. conceived the research and wrote the first draft of the paper. A.P.K. and M.J.R. designed the experimental approach. A.P.K. synthesized the materials and carried out the adsorption experiments. D.J.A. provided input on materials synthesis and characterisation. D.A., M.S.D., G.R.D. and N.G.B. designed the computational approach. D.A. performed the theoretical simulations. G.F.S.W. and E.J.C. performed the structural analyses. All the authors discussed the results and contributed to writing the manuscript. MJR directed the research.

Author information
Data availability
The data sets supporting findings of this study are available from the University of Liverpool, and can be found at doi:10.17638/datacat.liverpool.ac.uk/589.

Reprints
Reprints and permissions information is available at www.nature.com/reprints

Competing interests
The authors declare no competing financial interests.

Corresponding author
Correspondence and requests for materials should be addressed to rossein@liverpool.ac.uk.

Methods

Materials and reagents. $Zn(OAc)_2•2H_2O$ (99%), furfural, furfuryl alcohol, 1,4-dioxane, cyclopentanol, L-menthyl acetate and formamide were purchased from Sigma – Aldrich, H-Gly-Gly-L-His-OH (98%) from BACHEM, methanol, THF, DMSO and DMF from Fisher Chemical. All reagents and solvents were used without further purification.

Synthesis of ZnGGH-1•(DMF-H_2O). 1.5 mL of $Zn(OAc)_2•2H_2O$ aqueous solution (0.336 M), 0.9 mL of H-Gly-Gly-L-His-OH, GGH, aqueous solution (0.442 M), 1 mL of water and 10 mL of DMF were loaded into a 40 mL scintillation vial. The vial was heated at 90 ^oC for 48 h with a ramping rate of $1^oC.min^{-1}$ and cooled to room temperature at $0.5°C.min^{-1}$. Colorless crystals of ZnGGH-1•(DMF-H_2O) were produced in a yield of 75%. The term (DMF-H_2O) in the name of the material denotes the solvent used in the synthesis and contained in the pores.

Exchange of pore species in ZnGGH-1•(DMF-H_2O) for the synthesis of ZnGGH-2•(DMSO), ZnGGH-3•(DMF), ZnGGH-4•(H_2O), ZnGGH-4•(MeOH), ZnGGH-4•(Formamide), ZnGGH-5•(H_2O-DMF), ZnGGH-6•(F), ZnGGH-7•(FA) and ZnGGH-8•(THF). The remaining liquid after synthesis of ZnGGH-1•(DMF-H_2O) was decanted and the vial refilled with 15 mL of pure DMSO, DMF, H_2O, MeOH, formamide, furfural, furfuryl alcohol and THF or mixtures of them. The suspension was left under stirring for 24 hours at room temperature. A part of the obtained slurry (~ 100 μL) was transferred into a 1.0 mm capillary for PXRD analysis and the rest of the sample was filtered, washed with 8 mL of THF and dried on the Buchner funnel by the vacuum suction for 30 seconds. To obtain single crystals of the exchanged products, the as-made ZnGGH-1•(DMF-H_2O) crystals were soaked in the relevant solvent or guest systems at room temperature and shaken gently (150 rpm, on a Heidolph Vibramax 100 shaker) for 2 – 4 days. In the names of the materials, the molecule(s) in brackets denotes the liquid in which each exchange reaction was performed and is contained in the pores of the product.

Synthesis of ZnGGH-9. The collapsed structure ZnGGH-9 is produced by degassing ZnGGH-1 at 120^oC and 10^{-3} mbar for 12 hours. The same structure is formed by degassing of the exchanged structures (*e.g.,* ZnGGH-3•(DMF) and ZnGGH-4•(H_2O)).

Liquid guest adsorption experiments. 50 mg of ZnGGH-1•(DMF-H_2O) or ZnGGH-2•(DMSO) or ZnGGH-3•(DMF) or ZnGGH-4•(Formamide) were transferred in a 40 mL vial. Each vial was loaded with 0.1 mmol of a guest (dioxane, cyclopentanol, furfural, furfural alcohol) or with an equimolar mixture (0.1 mmol each) of a guest and the solvent that produces the ZnGGH structure under study (in case of ZnGGH-1•(DMF-H_2O) only DMF was used as solvent as it is the major component inside the pores of this material). For example, two adsorption experiments of dioxane on ZnGGH-2•(DMSO) were performed: the first used neat dioxane, and the second dioxane:DMSO 1:1 (molar ratio). Each suspension was left under stirring for 24 hours at room temperature. A part of the resulting slurry (~ 100 μL) was transferred into a 1.0 mm capillary for PXRD analysis and the rest of the sample was filtered, washed with 8 mL of THF and dried on the Buchner funnel by the vacuum suction for 30 sec. This protocol was developed to remove surface liquid and minimise volatilisation of the pore species, whereas washing with larger quantities of THF leads to removal of solvents and guests from the pores of ZnGGH. The species present in the pores were identified by ^1H NMR analysis of the digested sample in a DCl/d6-DMSO = 1/20 (v/v) solution.

Triggered adsorption experiments. Two vials were loaded with 50 mg of ZnGGH-2•(DMSO) and 0.1 mmol of one of the following liquid guests, dioxane (8.9 mL), cyclopentanol (9.06 mL) and L-menthyl acetate (24 mL). The suspensions were left under stirring at room temperature. After 24 h, 0.1 mmol of DMF (7.7 mL) was added to one of the vials and the suspensions were stirred for a further three days. Following this procedure a part

of the suspension slurry (~ 100 μL) was transferred into a 1.0 mm capillary for PXRD analysis, and the rest of the sample was filtered, washed with 8 mL of THF and dried on the Buchner funnel by the vacuum suction for 30 seconds. The species present in the pores were identified by ^{1}H NMR of the digested sample in a DCl/d_6-DMSO = 1/20 (v/v) solution. The guests were chosen based on the results of the individual adsorption experiments (see previous paragraph), in which dioxane and cyclopentanol were adsorbed by ZnGGH-1, ZnGGH-3 and ZnGGH-4. L-menthyl acetate was chosen as a liquid guest that is sufficiently large (minimum bounding box 5.2 x 10.2 x 10.6 Å) that it cannot diffuse through the pores of any of the ZnGGH-X structures (Supplementary Note 5).

Adsorption experiments on single crystals. Single crystals (~10 mg) of ZnGGH-2•(DMSO) were transferred in a vial loaded with 0.1 mmol (8.9 mL) of dioxane. The vial was shaken gently (150 rpm, on a Heidolph Vibramax 100 shaker) for 5 days, then crystals were collected from the vial to be analyzed by SCXRD. 0.1 mmol (7.7 mL) of DMF was added to the vial and the vial was shaken gently for 8 days, then crystals were collected and analyzed by SCXRD.

Triggered adsorption of dioxane – time course study. Four vials were loaded with 50 mg of ZnGGH-2•(DMSO) and 0.1 mmol dioxane (8.9 mL). After 24 h, 0.1 mmol of DMF (7.7 mL) was added to each vial. These experiments lasted for 1 hour, 6 hours, 1 day, and 2 days. At the end of each experiment a part of the suspension slurry was transferred into a 1.0 mm capillary for PXRD analysis, and the rest of the sample was filtered, washed with 8 mL of THF and dried on the Buchner funnel by the vacuum suction for 30 sec. The species present in the pores were identified by ^{1}H NMR of the digested sample in a DCl/d_6-DMSO = 1/20 (v/v) solution.

Triggered adsorption of dioxane with a reduced amount of DMF (DMF:dioxane = 1:2) . A vial was loaded with 50 mg of ZnGGH-2•(DMSO) and 0.1 mmol dioxane (8.9 mL). After 24 h, 0.05 mmol of DMF (3.85 mL) was added to the vial. Parts of the suspension slurry (~ 100 μL) were transferred into a 1.0 mm capillary for PXRD analysis after 4, 10 and 15 days. The rest of the sample was filtered, washed with 8 mL of THF and dried on the Buchner funnel by the vacuum suction for 30 sec after 15 days. The composition of the materials was identified by ^{1}H NMR of the digested sample in a DCl/d_6-DMSO = 1/20 (v/v) solution.

Powder X-ray diffraction (PXRD) patterns were collected in transmission geometry at room temperature with a D8 Advance Bruker diffractometer with Cu Kα_1 radiation (λ = 1.5406 Å). Samples in the form of powder or as a slurry in the solvents they were prepared from were transferred to a 1.0 mm internal diameter borosilicate capillary. Typically, profiles were collected as step scans over a 2 h period in the 5º< 2θ< 30º range with a step size of 0.025º. Synchrotron XRD powder patterns were collected on the I11 beam line at Diamond Light Source in 0.7 mm diameter borosilicate capillaries at 298 K. Data were collected using the Position Sensitive Detector (PSD, Mythen-2) in order to minimise data collection time and thus minimise exposure to the X-ray beam and any resulting beam damage. A pair of scans were collected and summed to account for gaps in the detector modules.

In situ PXRD investigation of the triggered adsorption of dioxane. A vial was loaded with 50 mg of ZnGGH-2•(DMSO) and 0.1 mmol dioxane (8.9 mL). After 24 h, 0.1 mmol of DMF (7.7 mL) was added to the vial. The suspension let under stirring for 1 min and a part of it was transferred into a 1.0 mm capillary for PXRD analysis. 80 profiles were collected as step scans over 20 hours in the 7.5º< 2θ< 15.5º range with a step size of 0.025º.

Nuclear magnetic resonance Solution phase ^{1}H NMR were collected on a 400 MHz Bruker instrument. Solid samples were digested in a DCl/d_6-DMSO = 1/20 (v/v) mixture.

Thermogravimetric analysis was carried out with a TA 500 instrument in the 25-700 ºC temperature range with a 10 ºC.min^{-1} scan rate and an air flow of 50 mL.min^{-1}. Evolved gas analysis was performed with a Hiden HAL IV RC RGA 201 mass spectrometer.

Single crystal X-ray diffraction (SCXRD) data for all structures were collected on a Rigaku MicroMax™-007 HF with a Mo Kα rotating anode microfocus source and a Saturn 724+

detector. Data integration and reduction were performed using CrysAlisPro. The structure was solved and refined using SHELX-20XX implemented using Olex2. Single crystal X-ray diffraction experiments were also performed at Diamond Light Source (beamline I19) using a Pilatus 2M detector and a 3-circle diffractometer using Zr-L edge wavelength (λ = 0.6889 Å). The data sets were collected to investigate disorder in the pores in certain ZnGGH structures.
Computational studies The dPCA analysis of linker conformations was performed in R using the package 'psych' (https://CRAN.R-project.org/package=psych). All DFT calculations, including energy minimization and Nudged Elastic Band (NEB) simulations,[31] were performed for a fully flexible three dimensionally periodic model of the ZnGGH unit cell using projector augmented wave (PAW)[32] method in the framework of the Generalised Gradient Approximation (GGA)[33] as implemented in the Vienna Ab initio Simulations Package (VASP)[34] version 5.3.5. The Perdew-Becke-Ernzerhof (PBE) functional was used for the simulations of an empty host. To take into account host-guest van der Waals interactions in the case where the pores were occupied we used the vdW-DF method[35] with the non-local exchange-correlation functional revPBE. We used an energy cut-off of 600 eV, Gaussian smearing of partial orbital occupancies with smearing width of 0.1 eV, the "accurate" precision setting with convergence criteria of $2x10^{-5}$ eV for the electronic energy convergence and 10^{-3} eV/Å for the residual force for the ionic convergence. The NEB calculations were set up using the recommended default VASP flags and settings. For each NEB trajectory, we used a total of eight system images including the two end images that were previously identified as local minima in steepest decent energy minimization calculations. The end points of each NEB trajectory in Figure 4(a) of the main text are shown as large coloured circles, while the six intermediate images are shown as smaller circles. All calculated points are interpolated by cubic splines to guide the eye.

Additional references

31 Sheppard, D., Terrell, R. & Henkelman, G. Optimization methods for finding minimum energy paths. *The Journal of Chemical Physics* **128**, 134106, (2008).

32 Blöchl, P. E. Projector augmented-wave method. *Physical Review B* **50**, 17953-17979, (1994).

33 Perdew, J. P., Burke, K. & Ernzerhof, M. Generalized Gradient Approximation Made Simple. *Physical Review Letters* **77**, 3865-3868, (1996).

34 Kresse, G. & Hafner, J. Ab initio molecular dynamics for liquid metals. *Physical Review B* **47**, 558-561, (1993).

35 Dion, M., Rydberg, H., Schröder, E., Langreth, D. C. & Lundqvist, B. I. Van der Waals Density Functional for General Geometries. *Physical Review Letters* **92**, 246401, (2004).